Dejiang Yang, Chun Wei*, Yongyang Gong*, Tianxi Liu and Jian Lv

Effects of preparation methods on the mechanical and thermal properties of graphene-modified HNBR composites

https://doi.org/10.1515/epoly-2017-0074
Received April 17, 2017; accepted September 5, 2017; previously published online October 18, 2017

Abstract: Polymers modified by graphene have become an attractive method to enhance the matrix properties, wherein the dispersion of graphene in the matrix and the interfacial interactions between graphene and matrix are critical to influence the final performance. In the present work, graphene nanosheet (GNS)-modified hydrogenated nitrile butadiene rubber (GNS/HNBR) composites were prepared via solution-mixing and mechanical-blending methods. The curing performance, mechanical properties and heat resistance of the prepared composites were studied. The results showed that when the content was 0.2 wt%, the tensile strength and modulus at 300% elongation of the GNS/HNBR composite prepared via solution-mixing method reached 19.36 and 3.62 MPa, which increased by 32% and 18% compared with those of pure HNBR, respectively. In addition, the swelling index of the composite in cyclohexane was decreased from 413% to 337%. On the other hand, the tensile property of GNS/HNBR composite prepared by mechanical-mixing method became poor. SEM observation showed that GNS was well dispersed and incorporated into HNBR via the solution-mixing method, resulting in a significant reinforcing effect.

Keywords: graphene nanosheet; hydrogenated nitrile butadiene rubber; mechanical blending; mechanical properties; solution mixing.

***Corresponding authors: Chun Wei and Yongyang Gong,** College of Materials Science and Engineering, Guilin University of Technology, Guilin 541004, P.R. China; and Ministry-Province Joint Base for State Key Laboratory of Processing for Non-ferrous Metals and Featured Materials, Guangxi Zhuang Autonomous Region, Nanning, China, e-mail: 1986024@glut.edu.cn (C. Wei); yygong@glut.edu.cn (Y. Gong)
Dejiang Yang and Jian Lv: Ministry-Province Joint Base for State Key Laboratory of Processing for Non-ferrous Metals and Featured Materials, Guangxi Zhuang Autonomous Region, Nanning, China
Tianxi Liu: College of Materials Science and Engineering, Guilin University of Technology, Guilin 541004, P.R. China; and Ministry-Province Joint Base for State Key Laboratory of Processing for Non-ferrous Metals and Featured Materials, Guangxi Zhuang Autonomous Region, Nanning, China

1 Introduction

Hydrogenated nitrile butadiene rubber (HNBR) has great mechanical properties, oil and heat resistance (1), and it has been widely used in automobiles and oil industries (2). Moreover, HNBR is well known for its thermal stability and usually replaced nitrile butadiene rubber (NBR) in the working place with high temperature or oxygen contents. In this kind of environment, thermal aging is the biggest threat to the service life of rubber products, and how to improve the aging and heat resistance and mechanic performance of rubber products is one of the important problems to be solved (3–5). Recent developments in oil and gas sectors require the products of HNBR having higher working temperature with uncompromised or even improved performances in mechanical properties, solvent resistance, sealing and so on.

In the last decade, the modification of HNBR has been vastly reported (6, 7), and layered material-reinforced HNBR has exhibited a better performance than conventional carbon-black reinforced one (8). For example, the layered structure of montmorillonite effectively hindered the growing of cracks in HBNR and improved the mechanical properties/sealing performance of HNBR materials, even in the presence of only 3–6 wt% montmorillonite (9). In addition, the layered structure of montmorillonite can form a protective layer in the material, which can impede the entry of gas molecules, greatly reducing the aging of rubber in a multi atmosphere environment.

Graphene contains one to several layers of graphene with a thickness of nanometer (10, 11), which have excellent mechanical properties, great electrical and thermal conductivities and huge specific surface area (12). Thus, compared with the montmorillonite, by using graphene to modify polymeric materials, their relevant properties can be enhanced simultaneously.

At present, there are many studies about using graphene-modified rubber (13–15), and the compound material is usually prepared by mechanical, solution or emulsion blending. Most attempts use graphene's high mechanical strength and modulus to enhance the mechanical properties of the rubber, or to endow it with versatile functions, such as electrical conduction, thermal conductivity, electromagnetic shielding and so on (16–20).

In addition, graphene nanostructures have large surface area and gas barrier property. The large-area and high-quality graphene has been fabricated out; however, it cannot be a filler material to enhance the polymers because of its expensive cost. The graphene nanosheets (GNSs) we used are prepared by mechanical method, and compared with the high-quality graphene, it may be a little bit cheaper. The GNS has the advantages of low cost, and mass production of GNS has been realized in China (21–25).

Many studies show that GNS as a filler-reinforced rubber improves the mechanical properties and heat resistance, and thermal aging is feasible in theory. Studies have shown that the GNS cannot be effectively exfoliated through mechanical blending (26). It is difficult to disperse the GNS in traditional mechanical blending, let alone the expected effects. The exfoliation and uniform dispersion of the GNS can be obtained by solution method, but there are many limitations because of the present environmental protection programs, such as usage of organic solvents, often toxic and highly flammable, and miscellaneous steps. Thus, there is no such product applied in industry yet because of the cost and practical results.

In this study, we combine the above-mentioned methods, prepare GNS/HNBR composites by solution method (masterbatch method) and attempt to fabricate high-performance composites in a low-cost way.

2 Experimental

2.1 Materials

HNBR (3446) was purchased from Lanxess (Germany). N,N-dimethylformamide (DMF) and dicumyl peroxide (DCP) were bought from Xilong Chemical Co., Ltd. (China). GNSs were supplied by Xingang Technologies Co., Ltd. (China). All chemicals and materials showed in the Table 1 were used without further treatment unless otherwise specified.

Table 1: Details of experimental materials.

Reagent or material	Specification	Source
HNBR (3446)	AR	Lanxess, Germany
N,N-dimethyl formamide	AR	Xilong Chemical Co., Ltd.
Dicumyl peroxide	AR	Xilong Chemical Co., Ltd.
Deionized water	Homemade	–
Graphene nanosheets	–	Xingang Technologies Co., Ltd.
Dicumylperoxid	AR	Xilong Chemical Co., Ltd.
Acetone	AR	Xilong Chemical Co., Ltd.

2.2 GNS/HNBR composites prepared with a solution-mixing method

As depicted in Figure 1, for pretreatment, 0.2 g of GNS was mixed with acetone and dried. The GNS was then mixed with DMF under stirring for 5 min at 20,000 rpm and then sonicated for 1 h. Twenty grams of HNBR was placed and dissolved in DMF. GNS/DMF was slowly added to HNBR/DMF under stirring. After 5 min, the solution was sonicated for 1 h, followed by further stirring for 3 h. Finally, a small amount of deionized water was added to precipitate the rubber, which was then repeatedly rinsed with ethanol for three times. The rinsed rubber was placed in an oven at 70°C until the weight was constant. Thus, the premixed GNS/HNBR was obtained.

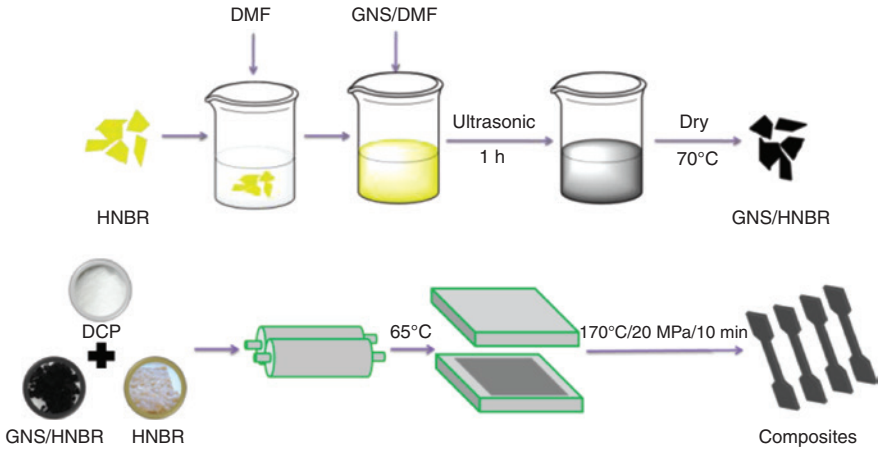

Figure 1: Preparation process of GNS/HNBR composites with the solution-blending method.

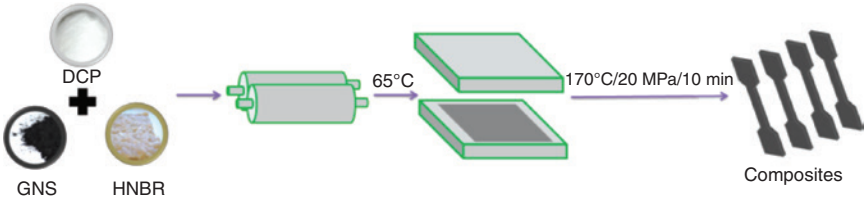

Figure 2: Preparation process of GNS/HNBR composites with the mechanical-blending method.

The premixed GNS/HNBR and pure HNBR were weighed separately at a GNS content 0.2, 0.4 and 0.6 wt%. These three mixtures were separately mixed with 3 wt% of DCP and blended mechanically on a roller mill. The temperature of the roller was set to be 65°C. After the rubber was rolled and placed for 6 h, a composite material was molded and cured under at 170°C under 10 MPa for 10 min. The molded and cured rubber was pressed into dog-bone-shaped specimens with a cutter.

2.3 GNS/HNBR composites prepared with a mechanical-blending method

As illustrated in Figure 2, pure HNBR (20 g), GNS (40 mg, 80 mg, 120 mg) and DCP (600 mg) were mechanically blended using a dual-roller mill at the temperature of 65°C. The rolled rubber was further placed for 6 h at room temperature and then molded and cured at 170°C under 10 MPa for 10 min. The cured rubber was finally pressed into dog-bone-shaped specimens.

2.4 Test and characterizations

X-ray diffraction (XRD) characterization was conducted with an X'Pert Pro X-ray diffractometer (PANalytical Co., Ltd., the Netherlands) from 5° to 50° at a scan speed of 5°/min. The source of X-ray was CuKα with a tube voltage of 40 kV and tube current of 40 mA. Scanning electron microscope (SEM) images of samples (coated with gold) were obtained with a JSM-6380LV SEM (JEOL Co., Ltd., Japan). The curing time and torque of samples were tested with a rotor-free curing instrument according to the Standard ISO 6502:1991. Tensile properties of the samples were tested with a UTM4000 computer-controlled electronic universal testing machine (Sansizongheng Technical Co., Ltd., Shenzhen City, China) according to the Standard ISO 37:1994. Thermogravimetric analysis (TGA) analysis was performed with a Q-500 TGA instrument (TA Co., Ltd., USA) from 25°C to 600°C at a heating rate of 10°C/min in nitrogen environment. Swelling resistance of the samples was evaluated according to the Standard GB-7763-81. (According to the characteristics of intelligent swelling and insoluble in cross-linked polymers in travel solvents, the samples were measured at constant temperature and mass ratio after swelling with preswelling.)

3 Results and discussion

3.1 Morphology of GNS after sonication

The SEM images of GNS powder and GNS dispersed in DMF after the ultrasonic treatment are shown in Figures 3A,B. In GNS powder, many layers of GNS were stacked together

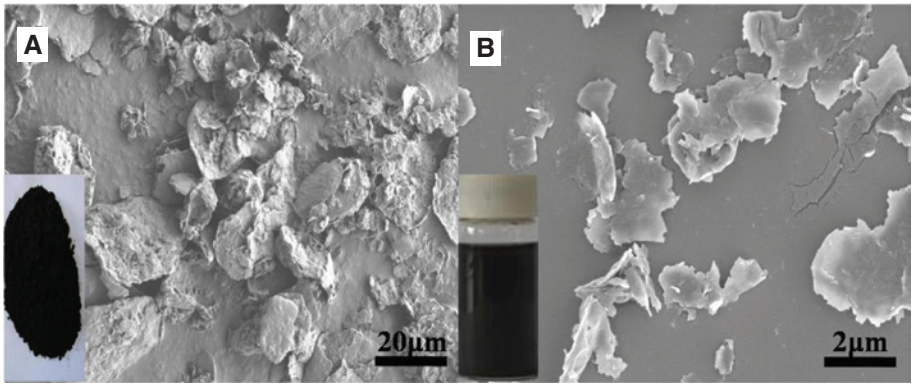

Figure 3: SEM images of (A) GNS powder and (B) GNS in DMF after the ultrasonic treatment (the insets are corresponding photographs).

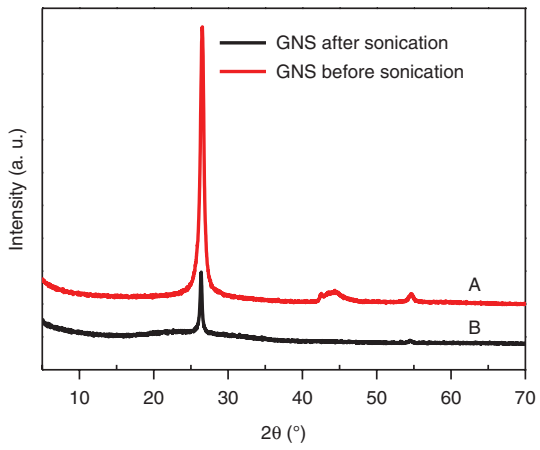

Figure 4: X-ray diffraction patterns of GNS before (A) and after (B) the sonication.

to form aggregates with the width of 20–30 μm. After the sonication, GNS was peeled off and stably dispersed in the DMF with thinner and smaller size (width of 2–4 μm), indicating the consequence of sonication processing.

In addition, XRD patterns of GNS before and after the sonication are measured and illustrated in Figure 4. The unpeeled GNS exhibited an intense characteristic peak at 25°. After the sonication, the intensity of the peak dramatically decreased, indicating that the sonication had exfoliated GNS sheets to some extent while at the same time broke them into small pieces (27, 28).

3.2 Dependence of the properties of GNS/HNBR composites on mixing methods

3.2.1 Dispersion of GNS in the composites

The SEM images of the rolled rubber prepared by the mechanical-blending method (M-GNS/HNBR) and solution-mixing method (S-GNS/HNBR) are illustrated in Figure 5A,B, respectively. The M-GNS/HNBR had large and stacked sheets with the width of 3–6 μm. The S-GNS/HNBR contained small and thin sheets, showing the uniform dispersion of GNS in the matrix of rubber. A contrast chart of the rolled rubber was prepared by two methods soaked in tetrahydrofuran (THF) solution. After 4 h, the supernatant was characterized by TEM. The TEM images of the GNS are illustrated in Figure 6C,D. The M-GNS/HNBR had large aggregates of GNS with the width of 1 μm, and the S-GNS/HNBR contained thin sheets.

For the M-GNS/HNBR, the shear stress between the rollers was not strong enough to break or peel the large stacked GNS sheets, resulting in poor dispersion status. By contrast, GNS was effectively peeled off and ruptured into small pieces by the sonication and well dispersed in HNBR to form S-GNS/HNBR.

3.2.2 XRD characterization of the composites

A characteristic peak of GNS ($2\theta = 26°$) was observed in the XRD patterns of the M-GNS/HNBR and S-GNS/HNBR (Figure 7). A broad diffraction peak was observed for HNBR ($2\theta = 19°$), indicating it is noncrystalline structure. The peak of S-GNS/HNBR was weaker than that of M-GNS/HNBR containing relatively large GNS crystals, and the full wave at half maximum (FWHM) bandwidth broadens, indicating that the shear stress in the mechanical-blending process was not stronger than that in sonication, and the periodic structure of GNS might be ruptured during ultrasonic process and GNS has been exfoliated into monolayers or few layers (29).

3.2.3 Curing performance of the composites

Both the maximum and the minimum torques (M_H, M_L) of the S-GNS/HNBR composite increased with the increase of

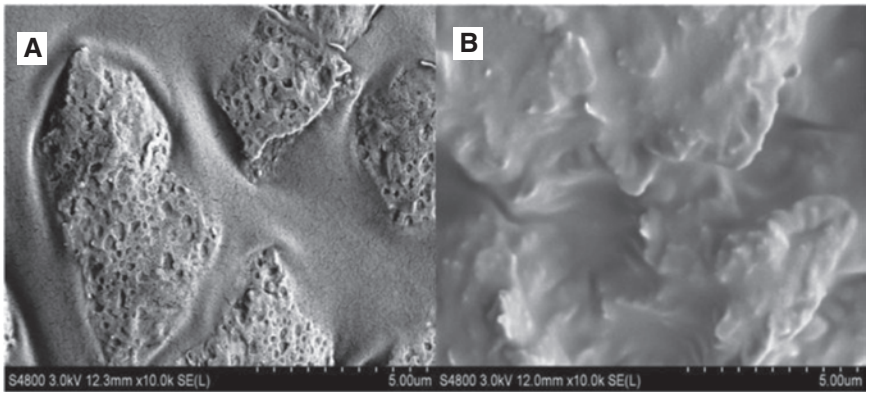

Figure 5: SEM images of (A) M-GNS/HNBR (B) S-GNS/HNBR.

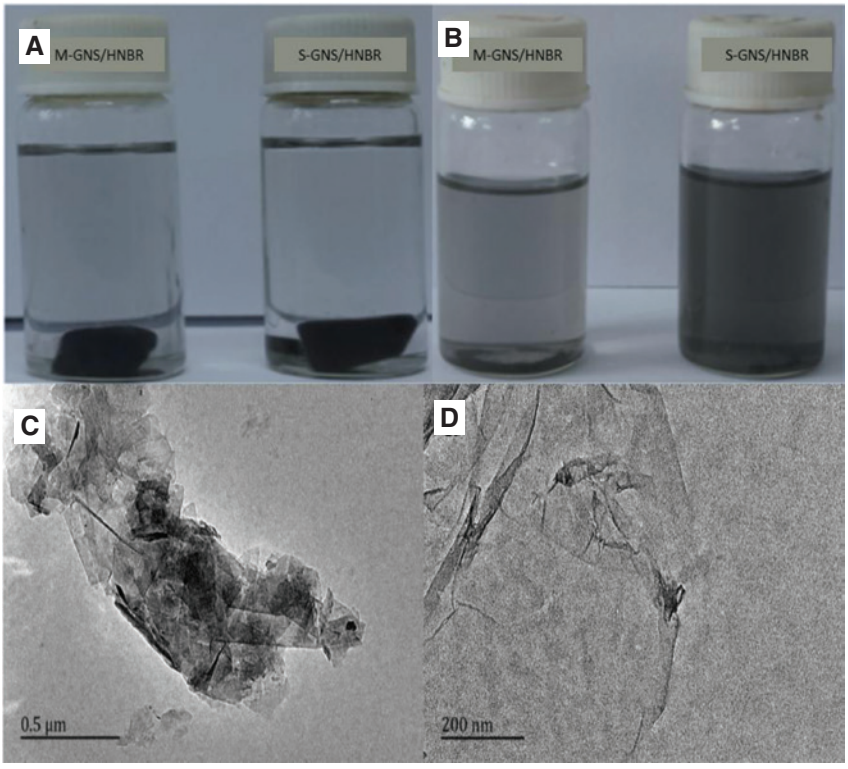

Figure 6: GNS/HNBR dissolve in the THF (A), and stand still for 4 h (B), TEM images of (C) M-GNS/HNBR (D) S-GNS/HNBR.

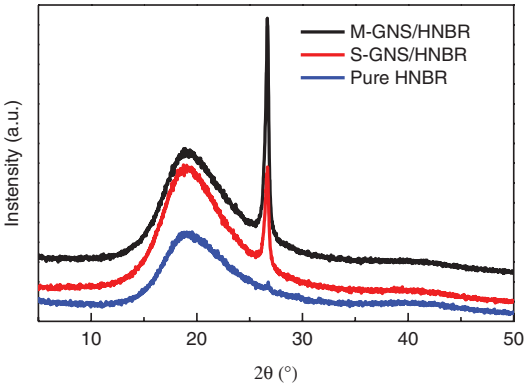

Figure 7: XRD patterns of the M-GNS/HNBR and S-GNS/HNBR composites.

GNS (Table 2), and the difference between the minimum and the maximum values was also increased, indicating that the cross-link density of the rubber was also increased. The curing time was shortened with an increasing content of GNS. The M-GNS/HNBR composite showed similar behaviors to a smaller extent. The reason could be the incorporation of thermally conductive GNS increased the thermal properties of the rubber, which facilitated the curing and shortened the scorch time and curing time. By contrast, the shear stress of the roller mill could not effectively peel and disperse GNS, resulting in the presence of GNS aggregates in the rubber. Consequently, no thermally conductive network structure could be formed, and thus the curing performance of M-GNS/HNBR hardly changed.

3.2.4 Mechanical properties of the composites

As can be seen from Table 3, the tensile strength and modulus at 300% elongation of the S-GNS/HNBR were significantly increased. At 0.2 wt% GNS, the tensile strength reached 19.36 MPa and modulus at 300% reached 2.73 MPa, which were 30.98% and 18.18% higher than those of pure HNBR, respectively. However, the M-GNS/HNBR with the same content of GNS had tensile strength of only 11.75 MPa, lower than that of pure HNBR by 20.5%.

The stress-strain behaviors of S-GNS/HNBR and M-GNS/HNBR are shown in Figure 8. As the GNS had high strength, high modulus and large specific surface area, the GNS was well dispersed in the matrix of S-GNS/HNBR. The great dispersion and resulting strong interactions improved the mechanical properties of S-GNS/HNBR. On the contrary, GNS was not fully peeled (see Figures 5 and 6) and poorly dispersed in the matrix of M-GNS/

Table 2: Curing performance of the GNS/HNBR composites.

Preparation method	Content of GNS (wt%)	M_H (Nm)	M_L (Nm)	$M_H - M_L$ (Nm)	T_{10} (s)	T_{90} (min)
Pure HNBR	0.0	3.390	0.298	3.091	25.2	4.24
Mechanical-blending method	0.2	6.569	1.002	5.567	17.4	2.45
	0.4	6.665	1.004	5.661	19.8	2.35
	0.6	6.599	1.152	5.513	20.4	2.29
Solution-blending method	0.2	5.062	0.403	4.659	23.6	3.45
	0.4	5.283	0.906	4.377	22.8	3.16
	0.6	5.484	2.057	3.427	14.4	2.52

Table 3: Mechanical properties of the GNS/HNBR composites.

Preparation method	Content of GNS (wt%)	Modulus at 100% elongation (MPa)	Modulus at 300% elongation (MPa)	Tensile strength (MPa)	Elongation at break (%)
Pure HNBR	0.0	1.31	2.31	14.78	457.40
Solution-blending method	0.2	1.34	2.73	19.36	467.75
	0.4	1.39	2.49	16.35	383.38
	0.6	1.47	3.62	15.17	426.10
Mechanical-blending method	0.2	1.38	3.38	11.75	402.51
	0.4	1.38	3.43	12.45	418.15
	0.6	1.44	3.66	12.59	387.33

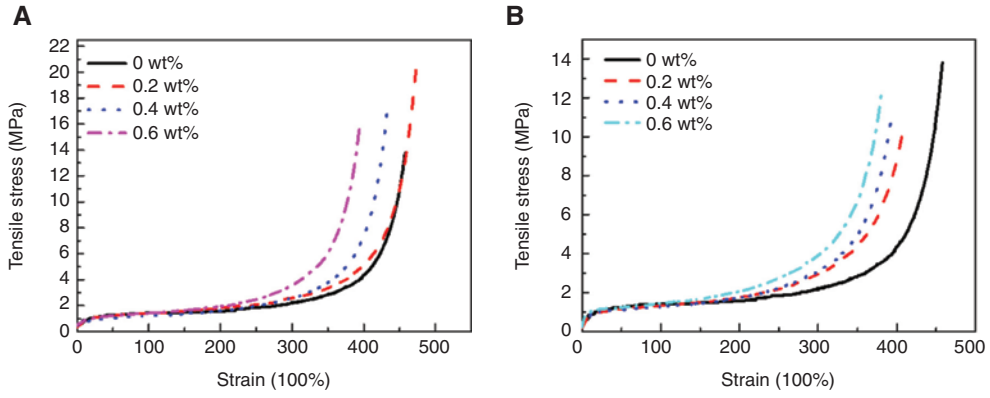

Figure 8: Typical stress-strain behavior of (A) S-GNS/HNBR and (B) M-GNS/HNBR.

HNBR. The added GNS was weakly bonded with the rubber at interfaces, leading to the absence of enhancing the effect of GNS and poor tensile performance of M-GNS/HNBR.

3.2.5 Thermal properties of the composites

The DTG profiles of GNS (0.4 wt%)/HNBR and HNBR are illustrated in Figure 9, and the temperatures at specific weight losses are described in Table 4. At the weight loss of 5% and 15%, the decomposition temperatures of M-GNS/HNBR (426°C and 450°C) and S-GNS/HNBR (428°C and 452°C) were only a little higher (even lower) than those of the pure HNBR (427°C and 449°C). By comparison, the DTG curve of M-GNS/HNBR and pure HNBR are nearly overlapping; the DTG curve of S-GNS/HNBR moves to the right with respect to the reference curves. The reason for the unimproved thermal stability is that the content of GNS was low or not fully peeled, and hence GNS could not form a lamellar network structure in the matrix. During the heating process of TGA, the evolution of small gas molecules could not be effectively impeded in the absence of the network structure.

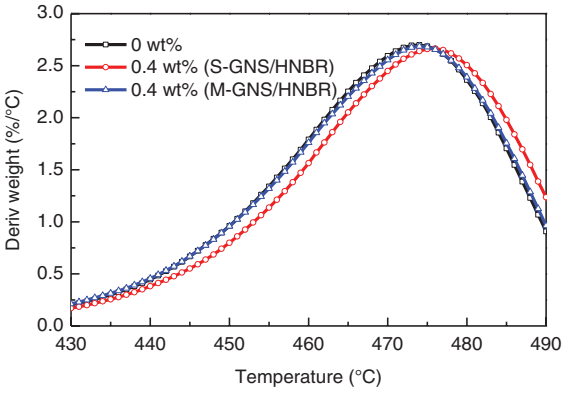

Figure 9: DTG profiles of GNS (0.4 wt%)/HNBR and HNBR.

Table 4: Decomposition temperatures of GNS (0.4 wt%)/HNBR and HNBR.

Preparation method	$T_{d5\%}$ (°C)	$T_{d15\%}$ (°C)	T_{max} (°C)
HNBR	427	449	473
M-GNS/HNBR	426	450	471
S-GNS/HNBR	428	452	475

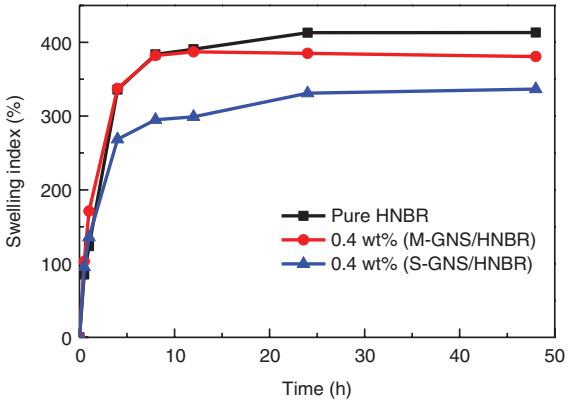

Figure 10: Plots of swelling indices of the composites against time.

3.2.6 Swelling resistance of the composites

The swelling indices of HNBR, S-GNS/HNBR and M-GNS/HNBR against soaking time (solvent: cyclohexane) are illustrated in Figure 10. The index of S-GNS/HNBR was the lowest (336.66% after the soaking time of 48 h), indicating that the dispersed lamellar GNS could effectively prevent the access of molecules of solvent into the gaps between the molecular chains of the rubber. Moreover, because of the large specific surface area of GNS sheets, GNS could be entangled with a portion of the molecular chains of the rubber, enhancing the resilience of the molecular chains and lowering the swelling index of the matrix. This effect was more significant in S-GNS/HNBR due to the effective peeling and great dispersion of GNS as discussed (30). For M-GNS/HNBR, the poor dispersion of GNS caused weak interfacial interactions between the GNS aggregates and the matrix of rubber. After the soaking process, the molecular chains of the rubber expanded, and the interfaces were loosened, resulting in the removal of GNS from the matrix. Accordingly, the swelling index declined after a long period of soaking.

3.2.7 Tensile fracture surfaces of the composites

The tensile fracture surface of S-GNS/HNBR was folded, and the peeled GNS sheets were 2–3 μm in width (Figure 11A). No cracks and aggregates were observed. On the contrary, most of the peeled GNS sheets on the tensile fracture surface of M-GNS/HNBR were large aggregates, and a large number of cracks were observed (Figure 11B).

According to the afore-mentioned experimental and characterization results, the mechanisms of tensile fracture of S-GNS/HNBR and M-GNS/HNBR are analyzed. In detail, GNS was well dispersed in the rubber matrix of S-GNS/HNBR and tangles with matrix molecular chain. It is not liable to cracks and peels off from the matrix in the

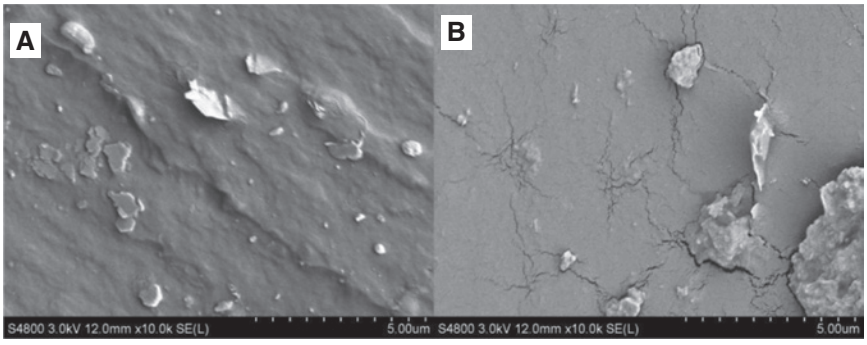

Figure 11: SEM images of the tensile fracture surfaces of (A) S-GNS/HNBR and (B) M-GNS/HNBR.

stretch process. The network cross-link point disperses the stress concentration, makes the rubber chain and gets the effective orientation and relaxation. In addition, GNS can effectively resist crack initiation and transfer the stress, leading to better mechanical properties. In M-GNS/HNBR, the dispersion of GNS was poor, and large aggregates were present. The cavitation and stress concentration were generated when the aggregates were loosened or removed by the tensile force, resulting in the formation of cracks neighboring the aggregates. The cracks caused the fracture of the material.

4 Conclusion

1. With the method of solution blending under sonication, GNS was effectively peeled and uniformly dispersed in HNBR. However, GNS was only slightly cracked (not peeled) by the shear stress in the mechanical-blending process.
2. With the increase of the content of GNS, the cross-link density and curing rate of S-GNS/HNBR increased more dramatically. At the content of GNS of 0.2 wt%, the tensile strength of S-GNS/HNBR reached 19.36 MPa, and modulus at 300% elongation reached 2.73 MPa, which increased by 30.98% and 18.18%, respectively, in contrast with pure HNBR.
3. The presence of GNS lowered the swelling index of HNBR, especially in S-GNS/HNBR. For instance, the swelling index of S-GNS (0.4 wt%)/HNBR was 336.66%, 18.5% lower than that of pure HNBR, after a soaking process in cyclohexane for 48 h.

Acknowledgments: The authors would like to gratefully acknowledge the generosity of the National Natural Science Foundation of China (grant no. 21264005), Guangxi Natural Science Foundation of China (grant no. 2014GXNSFAA118321, 2016GXNSFAA380029) and the Foundation of Guangxi Ministry-Province Jointly-Constructed Cultivation Base for State Key Laboratory of Processing for Non-Ferrous Metal and Featured Materials (13AA-6).

References

1. Huang A, Wang X, Jia D. Heat resistance and medium resistance properties of HNBR. China Elastomerics 2006:63–8.
2. Zhang J, Wang X, Zhang H, Sun Z. Molecular structure and properties of hydrogenated nitrile rubber. J Mater Eng. 2011:31–4.
3. Guo J. Advance in hydrogenated acrylonitrile-butadiene rubber. Chem Ind Eng Prog. 2001;20:31–4.
4. Hashimoto K, Watanabe N, Yoshioka A. Highly saturated nitrile new high temperature, chemical resistant elastomer. Rubber World 1984;190:32.
5. Nakagawa T, Toya T, Oyama M. Ozone resistance of highly saturated nitrile rubber (HNBR). J Elastom Plast. 1992;24: 240–61.
6. Lei C, Zhang L. Technical progress of blending modification of hydrogenated nitrile rubber. China Elastomerics 1998;3:43–7.
7. Psarras G, Sofos G, Vradis A, Anastassopoulos D, Georga S, Krontiras C, Karger-Kocsis J. HNBR and its MWCNT reinforced nanocomposites: crystalline morphology and electrical response. Eur Polym J. 2014;54:190–9.
8. Chen S, Yu H, Ren W, Zhang Y. Thermal degradation behavior of hydrogenated nitrile-butadiene rubber (HNBR)/clay nanocomposite and HNBR/clay/carbon nanotubes nanocomposites. Thermochim Acta. 2009;491:103–8.
9. Wang Y, Zhang L. Research on dispersed states of the bulking and strengthening agents in the rubber matrix. Journal of Beijing University of Chemical Technology (Natural Science Edition). 2000;27:10–4.
10. Gatos KG, Sawanis NS, Apostolov AA, Thomann R, KargerKocsis J. Nanocomposite formation in hydrogenated nitrile rubber (HNBR)/organo – montmorillonite as a function of the intercalant type. Macromol Mater Eng. 2004;289:1079–86.
11. Guo Y, Bao C, Song L, Yuan B, Hu Y. In situ polymerization of graphene, graphite oxide, and functionalized graphite oxide into epoxy resin and comparison study of on-the-flame behavior. Ind Eng Chem Res. 2011;50:7772–83.
12. Biswas S, Drzal LT. Multilayered nanoarchitecture of graphene nanosheets and polypyrrole nanowires for high performance supercapacitor electrodes. Chem Mater. 2010;22:5667–71.
13. Kuilla T, Bhadra S, Yao D, Joong Hee L. Recent advances in graphene based polymer composites. Prog Polym Sci. 2010;35:1350–75.
14. Rao CN, Sood AK, Subrahmanyam KS, Govindaraj A. Graphene: the new two-dimensional nanomaterial. Angew Chem Int Ed Engl. 2009;48:7752–77.
15. Bai X, Wan C, Zhang Y, Zhai Y. Reinforcement of hydrogenated carboxylated nitrile–butadiene rubber with exfoliated graphene oxide. Carbon 2011;49:1608–13.
16. Araby S, Zhang L, Kuan H-C, Dai J-B, Majewski P, Ma J. A novel approach to electrically and thermally conductive elastomers using graphene. Polymer 2013;54:3663–70.
17. Tang Y, Wang N, Yang F, Dai C. Preparation and characterization of modified graphene oxide/natural rubber composite by mechanical method. HighPolymer Materials Science&Engingeering. 2015:167–72.
18. Stankovich S, Dikin DA, Dommett GH, Kohlhaas KM, Zimney EJ, Stach EA, Piner RD, Nguyen ST, Ruoff RS. Graphene-based composite materials. Nature 2006;442:282–6.
19. Kim H, Miura Y, Macosko CW. Graphene/polyurethane nanocomposites for improved gas barrier and electrical conductivity. Chem Mater. 2010;22:3441–50.
20. Compton OC, Kim S, Pierre C, Torkelson JM, Nguyen ST. Crumpled graphene nanosheets as highly effective barrier property enhancers. Adv Mater. 2010;22:4759–63.
21. Wang ZL, Xu D, Wang H G, Wu Z, Zhang XB. In situ fabrication of porous graphene electrodes for high-performance energy storage. Acs Nano. 2013;7:2422–30.

22. Knieke C, Berger A, Voigt M, KluppTaylor RN, Röhrl J, Peukert W. Scalable production of graphene sheets by mechanical delamination. Carbon 2010;48:3196–204.
23. Duan M, Li S, Chen G. Research progress in preparation of graphene by mechanical exfoliation. J Mater Sci. 2013:85–91.
24. Niyogi S, Bekyarova E, Itkis ME, McWilliams JL, Hamon MA, Haddon RC. Solution properties of graphite and graphene. J Am Chem Soc. 2006;128:7720–1.
25. Zhan Y, Wu J, Xia H, Yan N, Fei G, Yuan G. Dispersion and exfoliation of graphene in rubber by an ultrasonically – assisted latex mixing and in situ reduction process. Macromol Mater Eng. 2011;296:590–602.
26. Singh VK, Shukla A, Patra MK, Saini L, Jani RK, Vadera SR, Kumar N. Microwave absorbing properties of a thermally reduced graphene oxide/nitrile butadiene rubber composite. Carbon 2012;50:2202–8.
27. Liang J, Huang Y, Zhang L, Wang Y, Ma Y, Guo T, Chen Y. Molecular-level dispersion of graphene into poly(vinyl alcohol) and effective reinforcement of their nanocomposites. Adv Funct Mater. 2010;19:2297–302.
28. Wang G, Yang J, Park J, Gou X, Wang B, Liu H, Yao J. Facile synthesis and characterization of graphene nanosheets. J Phys Chem C. 2008;112:8192–5.
29. Li D, Müller MB, Gilje S, Kaner RB, Wallace GG. Processable aqueous dispersions of graphene nanosheets. Nat Nanotechnol. 2008;3:101–5.
30. James H M, Guth E. Statistical thermodynamics of rubber elasticity. J Chem Phys. 1953;21:1039–49.